Chapter 23
Physico-chemical Characterisation of the Processes Involved in Enamel Remineralisation by CPP-ACP

Keith J. Cross, N. Laila Huq, Boon Loh, Li-Ming Bhutta, Bill Madytianos, Sarah Peterson, David P. Stanton, Yi Yuan, Coralie Reynolds, Glen Walker, Peiyan Shen, and Eric C. Reynolds

Abstract Casein phosphopeptides derived from tryptic digests of milk caseins spontaneously assemble with calcium and phosphate ions at high pH to form casein phosphopeptide-amorphous calcium phosphate complexes (CPP-ACP). These complexes have been shown to be able to repair lesions in tooth enamel (biohydroxyapatite – HA) both *in vitro* and *in vivo* (specifically white spot lesions in the early stages of tooth decay). In order to better understand the processes involved in enamel remineralisation, the chemical equilibria between the CPP and calcium and phosphate ions as a function of pH were investigated. Furthermore, a thin-enamel slab technique was developed with enhanced sensitivity to monitor the diffusion of radio-opaque ions into individual lesions over a period of days to weeks.

Keywords Enamel · CPP-ACP · Remineralisation · Hydroxyapatite · Diffusion · NMR · Model

23.1 Introduction

Dental caries is initiated by the action of plaque odontopathogenic bacteria that ferment dietary sugars and starches, thus producing organic acids that demineralise the subsurface of enamel hydroxyapatite (Robinson et al. 2000). Since enamel caries is

K. J. Cross · N. L. Huq · B. Loh · L.-M. Bhutta · B. Madytianos · S. Peterson · D. P. Stanton
Y. Yuan · C. Reynolds · G. Walker · P. Shen · E. C. Reynolds (✉)
Oral Health Cooperative Research Centre, Melbourne Dental School,
Bio21 Institute of Molecular Science and Biotechnology, The University of Melbourne,
Melbourne, VIC, Australia
e-mail: keith.cross@unimelb.edu.au; laila@unimelb.edu.au; billym@student.unimelb.edu.au; speterson1@student.unimelb.edu.au; dstanton@unimelb.edu.au; yuay@unimelb.edu.au; coralie@unimelb.edu.au; gdwalker@unimelb.edu.au; peiyan@unimelb.edu.au; e.reynolds@unimelb.edu.au

K. Endo et al. (eds.), *Biomineralization*,
https://doi.org/10.1007/978-981-13-1002-7_23

[1] Arg[1]-Glu-Leu-Glu-Glu-Leu-Asn-Val-Pro-Gly-Glu-Ile-Val-Glu-Ser(*P*)-Leu-(Ser(*P*)-)$_3$(Glu-)$_2$-Ser-Ile-Thr-Arg[25] β-CN(1-25)

[2] Gln[59]-Met-Glu-Ala-Glu-Ser(*P*)-Ile-(Ser(*P*)-)$_3$(Glu-)$_2$-Ile-Val-Pro-Asn-Ser(*P*)-Val-Glu-Gln-Lys[79] α_{S1}-CN(59-79)

[3] Asn[46]-Ala-Asn-Glu-Glu-Glu-Tyr-Ser-Ile-Gly-(Ser(*P*)-)$_3$(Glu-)$_2$-Ser(*P*)-Ala-Glu-Val-Ala-Thr-Glu-Glu-Val-Lys[70] α_{S2}-CN(46-70)

[4] Lys[1]-Asn-Thr-Met-Glu-His-Val-(Ser(*P*)-)$_3$(Glu-)$_2$-Ser-Ile-Ile-Ser(*P*)-Gln-Glu-Thr-Tyr-Lys[21] α_{S2}-CN(1-21)

Fig. 23.1 Sequences of the predominant tryptic phosphopeptides of CPP-ACP in three-letter code. The cluster sequence motif critical to calcium and phosphate binding is highlighted in red

essentially a chemical process, at early stages of dental caries, the hydroxyapatite mineral loss is reversible. Any products that prevent enamel demineralisation and promote remineralisation are described as exhibiting anticaries activity. The principal components of dairy products associated with their anticariogenic activity are multi-phosphorylated caseins complexed with calcium and phosphate. Enzymic hydrolysis of caseins yields phosphopeptides known as casein phosphopeptides (CPP). These peptides, with their multiple phosphoseryl residues, bind relatively large quantities of calcium and phosphate ions in an amorphous, bioavailable form (Reynolds et al. 1995). The resulting complexes are known as casein phosphopeptide-amorphous calcium phosphate (CPP-ACP). The two dominant, self-assembling peptides are β-CN(1-25) and α_{S1}-CN(59-79) forming 20–30% by mass of the total CPP (Fig. 23.1). These bovine casein-derived peptides all contain the cluster sequence motif -(Ser(*P*)-)$_3$(Glu-)$_2$.

The aim of this study was to investigate the interactions between the peptides and crystalline and non-crystalline mineral components during the remineralisation process.

23.2 Materials and Methods

23.2.1 Materials

Extracted human third molars were obtained from patients attending the Melbourne Dental School with ethics approval (1340048). Enamel slices (~300 μ thick) were prepared from these teeth for examination.

23.2.2 Ion-Binding Studies

To evaluate the influence of pH on the calcium and phosphate ion equilibria, solutions of CPP-ACP, α_{S1}-CN(59-79)-ACP, and β-CN(1-25) were subjected to pH titrations. Calcium and phosphate ion concentrations were determined using microfiltration using previously described protocols, (Cross et al. 2005) modified to use a Dionex ion analyser.

23.2.3 Nuclear Magnetic Resonance Studies

NMR spectra were acquired at 599.741 MHz on a Varian Unity Inova spectrometer as described previously (Cross et al. 2016). Solution-phase diffusion measurements were performed using the sLED experiment as described previously (Altieri et al. 1995).The amplitude of the NMR signal is a function of the applied magnetic field gradient and the Stokes-Einstein radius of the diffusing species ($S \propto \exp(-\alpha D G^2)$,where D is the diffusion coefficient, G is the magnetic field gradient, and α depends on experimental values. The diffusion coefficient is related to the hydrodynamic radius by $D = k_B T/6\pi\rho R$ where k_B is the Boltzmann constant, T the absolute temperature, ρ the solution viscosity, and R the hydrodynamic radius of the spherical particles.

23.2.4 Remineralisation Studies

The novel technique utilised thin slabs of enamel (~300 μ thick) cut from human third molars that allowed sound mineral portions of the slabs to be used as controls in measuring the time course of remineralisation of artificial lesions. The technique is an extension of that previously described (Cochrane et al. 2008), with remineralisation of individual slabs being assessed after 0, 2, 3, 6, 12, 15, and 20 days immersion in a remineralisation solution at either pH 5·5 or pH 7·0. Diffusion of radio-opaque ions into the artificially prepared lesions was monitored by TWIM (Thomas et al. 2006). Acid-resistant nail polish was used to define the remineralisation zone and applied three times to prevent leakage during the soaking in the remineralisation solutions. Remineralising solutions consisted of 1% solutions of either CPP-ACP or β-CN(1-25)-ACP prepared at either pH 7.0 or 5.5 to compare the effects of neutral and acidic pH.

Lesion-sections were subjected to transversal wavelength-independent microradiography (TWIM) at days 0, 2, 3, 6, 12, 15, and 20 to visualise the time dependence of mineral ion uptake during enamel remineralisation. Microradiographs acquired on day 0 were used as control images for each lesion-section. The

lesion-sections remained soaked in the remineralisation solutions except when being X-rayed.

DOSY experiments were performed using the sLED technique to determine the relative rates of diffusion of the complexes using either the integrated aromatic or aliphatic signals of a β-CN(1-25)-ACP sample.

SDS-PAGE of CPP cross-linked using glutaraldehyde was conducted to analyse the multimerisation of CPP as described previously (Cross et al. 2016).

23.3 Results

23.3.1 The CPP-ACP Complexes Exist in Equilibria with Both Bound and Free Calcium and Phosphate Ions

When prepared at pH 9, the CPP-ACP complexes have most of the calcium and phosphate peptide bound. However, these complexes exist in solution in equilibrium with free ionic calcium and phosphate. Figure 23.2 shows sigmoidal pH titration curves for β-CN(1-25)-ACP representative of results obtained in this study. The pK_a values for Ca^{2+} and Pi binding are 5.983 ± 0.038 and 6.302 ± 0.067, respectively.

Further pH titrations were performed on 1% and 2% β-CN(1-25)-ACP complexes prepared with varying Ca/Pi ratio and varying peptide:Ca ratio. Plots of the bound calcium and phosphate concentrations against pH revealed sigmoidal curves whose shape remained independent of the Ca/Pi ratio. For the complexes prepared at ratios of Ca/Pi ranging from 1.6 to 1.51, and 12–15 Ca/peptide, the pH dependence

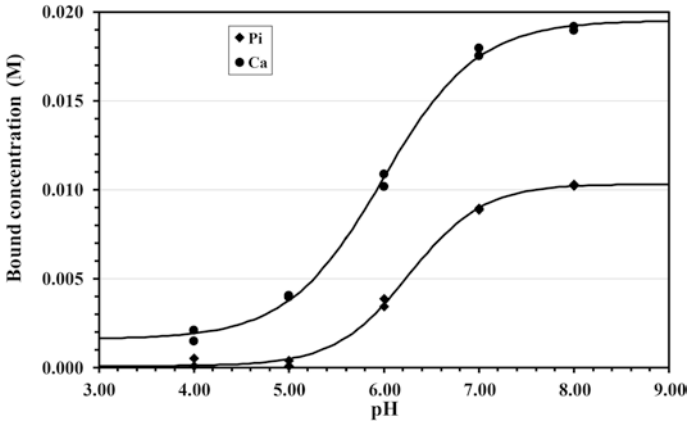

Fig. 23.2 Representative pH titration curves for a laboratory-prepared sample of β-CN(1-25)-ACP. The solid-line curves are fit to the Henderson-Hasselbalch formula yielding effective pK_a values of 6.302 ± 0.067 for the phosphate ion curve and 5.983 ± 0.038 for the calcium ion curve. Note that at low pH, the peptides bind residual calcium ions but no phosphate ions

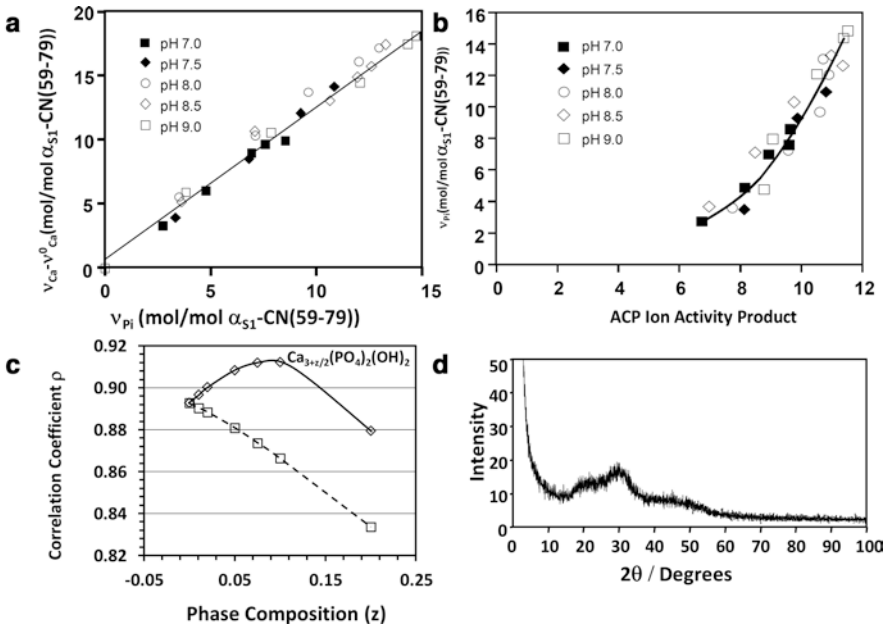

Fig. 23.3 (**a**) A plot illustrating the linear relationship between CPP-bound inorganic phosphate and CPP-bound calcium in excess of that bound at low pH (denoted by ν^0_{Ca}). (**b**) A plot of CPP-bound inorganic phosphate against ACP ion activity product. This illustrates that only an amorphous calcium phosphate phase predicts a one-to-one functional dependence of calcium phosphate ion activity product and the activity of phosphate (shown here) or calcium. (**c**) A plot illustrating that the best fit between the ion activity product and the phosphate (or calcium) activity occurs with a slightly calcium-rich, non-stoichiometric ACP phase having the formula $Ca_{3.0425}(PO_4)_2(OH)_{0.085}$. The lower curve is for calcium-deficient ACP phases and does not have a maximum at realistically achievable compositions. (**d**) X-ray powder diffraction image of a CPP-ACP sample demonstrating the broad peaks expected from an amorphous solid

of the bound calcium and phosphate were similar. Further analysis using α_{S1}-CN(59-79)-ACP revealed a well-defined phase of ACP stabilised by the CPP (Fig. 23.3a–c). Figure 23.3d shows a representative powder X-ray diffraction pattern of CPP-ACP that is consistent with an amorphous phase of calcium phosphate.

23.3.2 The CPP-ACP Complexes Are Small Readily Diffusible Species

The sLED experiment yields a diffusion-dependent signal whose functional dependence on the applied, magnetic-field gradient is dependent on the hydrodynamic radius of the molecule being studied. Figure 23.4a shows a plot of sLED signal intensity against the applied magnetic field gradient. This provides the ratio of hydrodynamic radii of the β-CN(1-25)-ACP complex relative to that of water. The

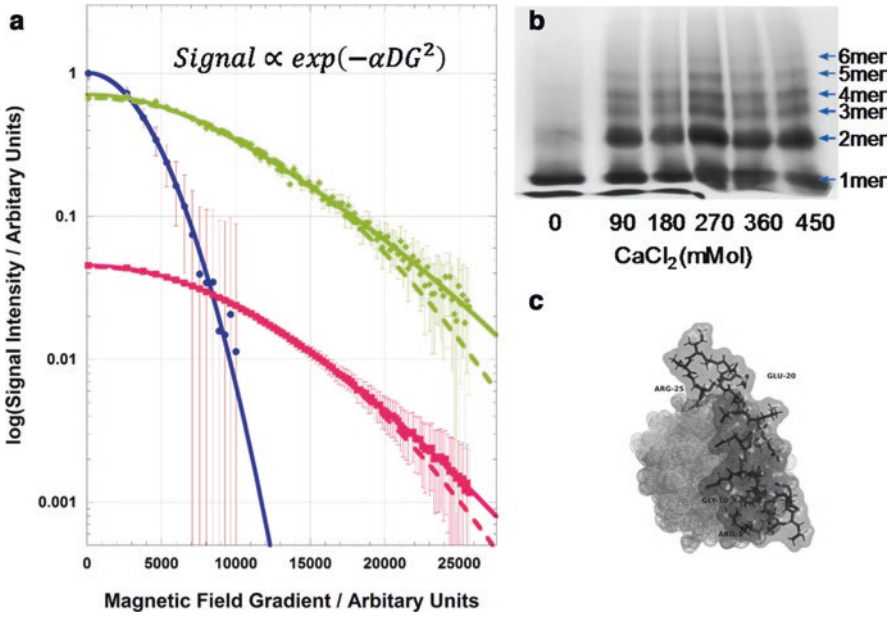

Fig. 23.4 (**a**) A representative plot of data from the sLED NMR experiment (Altieri et al. 1995) that uses magnetic field gradients to measure the relative rates of diffusion of various protonated species. The water signal (blue) can be compared with either the integrated aromatic (green) or aliphatic (red) signals of a CPP-ACP sample. The data from both peptide curves provided an internal consistency check. The Stokes-Einstein equation relates the hydrodynamic radius of a particle and its diffusion constant, allowing the determination of the hydrodynamic radius of the complexes given the known radius of water. The calculated hydrodynamic radii of the CPP-ACP complexes ranged from 1.53 ± 0.03 nm at pH 6 to 1.92 ± 0.08 nm at pH 9. The deviation from the fitted curves at high-magnetic-field-gradient values fits a two-component model consistent with the formation of aggregates. (**b**) A representative SDS-PAGE gel featuring the cross linking of the CPP using glutaraldehyde, observed in the presence of calcium ions. The multimerisation was also observed in the presence of calcium and phosphate ions suggesting that the complexes contain up to six CPP peptides. (**c**) A model of the CPP-ACP complex consistent with these and various other experiments. The peptide is depicted as sticks within a translucent van der Waals surface, and the ACP is shown as a pale grey van der Waals surface

measured hydrodynamic radii of the β-CN(1-25)-ACP complex range from 1.53 ± 0.03 nm at pH 6 to 1.92 ± 0.08 nm at pH 9. The deviation from the fitted curves at high-magnetic-field-gradient values fits a two-component model that is consistent with the formation of aggregates.

SDS-PAGE of CPP cross-linked using glutaraldehyde, in the presence of either calcium ions (Fig. 23.4b) or calcium and phosphate ions (Cross et al. 2016), suggests that the complexes contain up to six CPP peptides. Figure 23.4c shows a model of the CPP-ACP complex consistent with the results of these experiments.

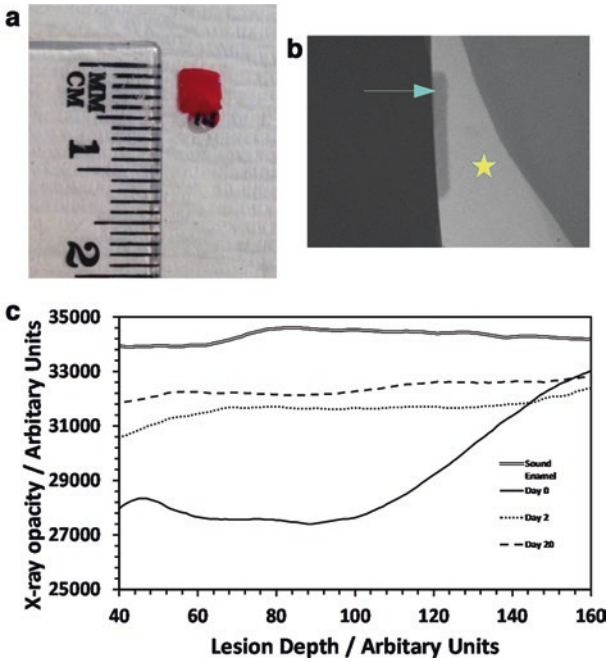

Fig. 23.5 Key features of the developed method to study the time dependence of remineralisation of enamel using thin slabs of enamel (~300 μ) cut from human third molars. The sound enamel regions provide the experimental control regions for the experiments. (**a**) Thin slab of enamel cut from human third molar and prepared with acid-resistant nail polish defining the remineralisation zone. (**b**) X-ray micrograph showing demineralised zone (arrow) and adjacent sound enamel (star). (**c**) Time-dependent, X-ray opacity of a specific enamel slab demonstrating diffusion of mineral ions into the lesion. Remineralisation occurs within a few days. This plot of X-ray opacity against lesion depth enables the calculation of A_s being the area under the sound enamel curve, A_m representing the areas under the individual 'remineralised' enamel curves, and A_d being the area under the 'demineralised' enamel curve (day 0) to determine extent of remineralisation (see Fig. 23.6)

23.3.3 Both CPP-ACP and β-CN(1-25)-ACP Complexes Release Mineral Ions that Remineralise Demineralised Enamel Lesions

Blocks of enamel from third molars with demineralised lesions were prepared that yielded multiple uniformly demineralised lesion-sections that would enable inter-tooth and intra-tooth comparisons (Fig. 23.5a). The sound enamel regions provided the experimental control regions for the experiments. Acid-resistant nail polish was used to define the remineralisation zone. Microradiography was used to visualise the time dependence of mineral ion uptake, in enamel remineralisation experiments. Figure 23.5b shows a sample X-ray micrograph with the demineralised zone (arrow) and the adjacent sound enamel (star).

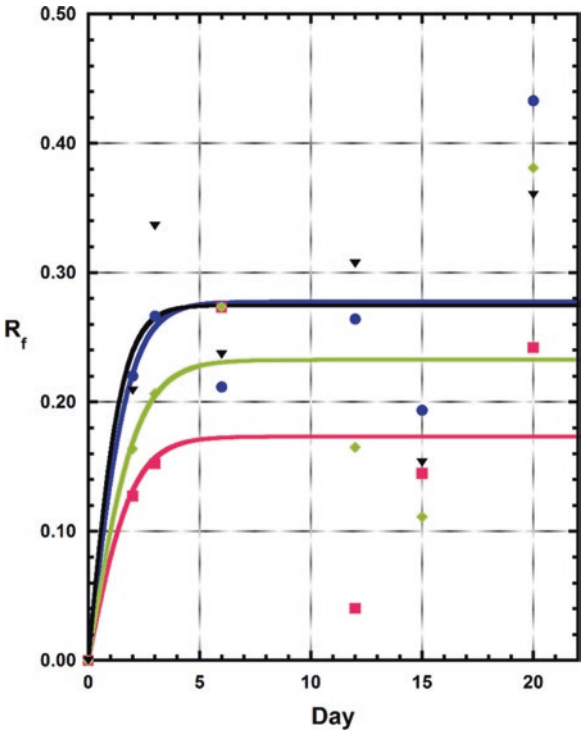

Fig. 23.6 Plot of time-dependent remineralisation for four lesion-sections. Each data point represents the extent of remineralisation calculated by the ratio $R_f = \frac{A_m - A_d}{A_s - A_d}$, where A_m is the area under the 'remineralised' enamel curve, A_d is the area under the 'demineralised' enamel curve (day 0), and A_s is the area under the sound enamel curve. Statistically significant differences in the extent of remineralisation are observed between different samples and may be due to biological differences: the lowest R_f of 0.17 ± 0.04 (in the graph above) differs significantly from the maximum R_f of 0.28 ± 0.04 at a $p = 0.025$

Figure 23.5c shows a plot of the time-dependent, X-ray opacity of a specific enamel slab after demineralisation at day 0 and following remineralisation until day 20. The X-ray data showed a diffusion-dependent increase in electron density, interpreted as mineralisation.

A time-dependent uptake of mineral was observed in the presence of both CPP-ACP and β-CN(1-25)-ACP at both pH values. The calculated data from each sample was fitted to the time-dependent part of a diffusion equation of the form

$$R_f = R_{f_{\max}} \times \tanh(kt)$$

where 'k' represents the rate constant for diffusion and 't' represents the elapsed time taken in days. The Pearson correlation coefficients for the non-linear curve fit confirmed that the data were consistent with a simple diffusion model for remineralisation. Figure 23.6 illustrates time-dependent plots of the calculated extent of remineralisation (R_f) for four representative sections. The data is consistent with mineral ions from CPP-ACP and β-CN(1-25)-ACP diffusing into and interacting with the enamel crystals. A recent study of the interaction of CPP-ACP with either enamel or saliva-coated enamel (Huq et al. 2018) indicates that chemical

equilibrium is established within a few hours; thus, the rate-limiting step for enamel remineralisation is the rate of diffusion of ions into the subsurface enamel.

23.4 Discussion

In this study, a variety of methods have been used to characterise the complexes formed by the casein phosphopeptides with calcium and phosphate ions. CPP bind calcium and phosphate to form stable CPP-ACP complexes in alkaline solution. These studies show that the ratio of bound calcium to bound phosphate is constant and independent of pH in the range of pH 7–9. Furthermore, the ion activity product fits a single curve for a calcium-rich, non-stoichiometric calcium phosphate phase. DOSY experiments using the sLED sequence demonstrated that the complex has a small but significant variation in size with pH. These experiments further revealed the ability of the small complexes to aggregate as concentrations were increased. The model of the CPP-ACP complex with all amino acids in the peptides interacting with the ACP surface is consistent with earlier findings that the peptide length influences the extent of binding to calcium and phosphate ions (Cross et al. 2005).

The importance of small readily diffusible CPP-ACP complexes is confirmed by the experiments using thin slabs of human enamel with artificial lesions that mimic early carious lesions. To enable the time-dependent monitoring, the current remineralisation procedures (Shen et al. 2011) required extensive improvements. The use of the single section for all-time points required a thicker section to withstand repeated handling. To accommodate the increased thickness, TWIM was used instead of the commonly used transverse microradiography (TMR) technique, both methods being validated techniques for monitoring carious lesions (Thomas et al. 2006). In addition, the acid-resistant nail varnish was reapplied three times to prevent leakage during the soaking in remineralisation solutions. To improve the signal-to-noise ratio, an additional 500-μ-thick aluminium filter was used with an optimal X-ray tube voltage of 30 kV.

We observed statistically significant differences in the extent of remineralisation within the multiple lesion-sections derived from the same individual tooth. These differences were attributed to varying microporosities of the demineralised lesion-sections of each individual tooth.

In conclusion, the CPP-ACP complexes were characterised to be a small readily diffusible species that can release the mineral ions on contact with demineralised enamel lesions. Furthermore both CPP-ACP and β-CN(1-25) complexes were able to remineralise within a few days in in vitro experiments.

Acknowledgements This study was funded by the Oral Health Cooperative Research Centre and NHMRC. Extracted human third molars were obtained from patients attending the Melbourne Dental School with ethics approval (1340048).

References

Altieri AS, Hinton DP, Byrd RA (1995) Association of biomolecular systems via pulsed field gradient NMR self-diffusion measurements. J Am Chem Soc 117(28):7566–7567

Cochrane NJ, Saranathan S, Cai F, Cross KJ, Reynolds EC (2008) Enamel subsurface lesion remineralisation with casein phosphopeptide stabilised solutions of calcium, phosphate and fluoride. Caries Res 42(2):88–97. https://doi.org/10.1159/000113161

Cross KJ, Huq NL, Palamara J, Perich JW, Reynolds EC (2005) Physicochemical characterization of casein phosphopeptide-amorphous calcium phosphate nanocomplexes. J Biol Chem 280(15):15362–15369

Cross KJ, Huq NL, Reynolds EC (2016) Casein phosphopeptide-amorphous calcium phosphate nanocomplexes: a structural model. Biochemistry 55(31):4316–4325. https://doi.org/10.1021/acs.biochem.6b00522

Huq NL, Cross KJ, Myroforidis H, Stanton DP, Chen YY, Ward BR, Reynolds EC (2018) Molecular interactions of peptide encapsulated calcium phosphate delivery vehicle at enamel surfaces. Proc BIOMIN XIV

Reynolds EC, Cain CJ, Webber FL, Black CL, Riley PF, Johnson IH, Perich JW (1995) Anticariogenicity of calcium phosphate complexes of tryptic casein phosphopeptides in the rat. J Dent Res 74(6):1272–1279

Robinson C, Shore RC, Brookes SJ, Strafford S, Wood SR, Kirkham J (2000) The chemistry of enamel caries. Crit Rev Oral Biol Med 11(4):481–495

Shen P, Manton DJ, Cochrane NJ, Walker GD, Yuan Y, Reynolds C, Reynolds EC (2011) Effect of added calcium phosphate on enamel remineralization by fluoride in a randomized controlled in situ trial. J Dent 39(7):518–525. https://doi.org/10.1016/j.jdent.2011.05.002

Thomas RZ, Ruben JL, de Vries J, ten Bosch JJ, Huysmans MC (2006) Transversal wavelength-independent microradiography, a method for monitoring caries lesions over time, validated with transversal microradiography. Caries Res 40(4):281–291